

# Kinematics of Galaxies in the Hubble Deep Field South: Discovery of a Very Massive Spiral at $z=0.6$ <sup>1</sup>

D. Rigopoulou<sup>1</sup>, A. Franceschini<sup>2</sup>, H. Aussel<sup>3</sup>, R. Genzel<sup>1</sup>, N. Thatte<sup>1</sup>, C.J. Cesarsky<sup>4</sup>

## ABSTRACT

We report the first results from a study of the internal kinematics, based on spatially resolved  $H_\alpha$  velocity profiles, of three galaxies at redshift  $z \sim 0.6$  and one at redshift  $z \sim 0.8$ , detected by ISOCAM in the Hubble Deep Field South. The kinematics are derived from high resolution near-infrared VLT spectroscopy. One of the galaxies is a massive spiral which possesses a very large rotational velocity of  $460 \text{ km s}^{-1}$  and contains a mass of  $10^{12} M_\odot$  (within 20 kpc), significantly higher than the dynamical masses measured in most other local and high redshift spirals. Two of the galaxies comprise a counter-rotating interacting system, while the fourth is also a large spiral. The observed galaxies are representative examples of the morphologies encountered among ISOCAM galaxies. The mass-to-light ( $M/L_{bol}$ ) ratios of ISOCAM galaxies lie between those of local luminous IR galaxies and massive spirals. We measure an offset of  $1.6 \pm 0.3 \text{ mag}$  in the rest frame B-band and of  $0.7 \pm 0.3 \text{ mag}$  in the rest frame I-band when we compare the four ISOCAM galaxies to the local Tully-Fisher B and I-band relations. We conclude that the large IR luminosity of the ISOCAM population results from a combination of large mass and efficient triggering of star formation. Since ISOCAM galaxies contribute significantly to the Cosmic Infrared Background our results imply that a relatively small number of very massive and IR luminous objects contribute significantly to the IR background and star formation activity near  $z \sim 0.7$ .

*Subject headings:* galaxies: evolution - galaxies: starburst - cosmology: observations

---

<sup>1</sup>Max-Planck-Institut für extraterrestrische Physik, Postfach 1312, 85741 Garching, Germany

<sup>2</sup>Dipartimento di Astronomia, Università di Padova, Vicolo Osservatorio 5 I-35122, Padova, Italy

<sup>3</sup>Institute for Astronomy, 2680 Woodlawn Drive, Honolulu, Hawaii, 96822, USA

<sup>4</sup>European Southern Observatory, Karl-Schwarzschild-str. 2, 85740 Garching, Germany

<sup>1</sup>Based on observations collected at the European Southern Observatory, Chile, ESO Nos 65.O-0612, 67.A-0518

## 1. Introduction

Most studies of high redshift galaxies have targeted their statistical properties such as galaxy counts, colors and redshift distributions (e.g. Koo & Kron 1992; Lilly et al. 1995). The information obtained this way has been used to construct the luminosity function which when compared with various models can give us clues about the evolution of galaxies at earlier epochs (e.g. Gronwall & Koo 1995). The advent of 10m class telescopes combined with advances in detector technology offers the possibility of a more detailed investigation of the high redshift population aimed at better understanding their physical properties and internal kinematics, the latter being ultimately related to the question of their evolution. Such a detailed study of the internal kinematics of high-redshift systems has the advantage of studying the evolution of galaxies on a galaxy by galaxy basis, in contrast to redshift surveys that study a large sample of similar but not exactly identical galaxies and derive “mean” properties that are then applied to the entire sample.

However, measuring the evolution of mass/luminosity of high-redshift galaxies directly is a challenging task. The Faber-Jackson relation for spheroid-dominated systems (Faber & Jackson 1976) and the Tully-Fisher relation for spiral galaxies (Tully & Fisher 1977, TF) are important tools for investigating galaxy kinematics. By comparing high-redshift galaxies with morphologically similar local galaxies we can study fundamental properties of the high- $z$  systems, investigate the processes by which disk-formation occurs (e.g. Navarro & Steinmetz 2000; Mo & Mao 2000) and eventually understand galaxy formation. Internal kinematic information is crucial since it provides a direct estimate of the masses of galaxies and allows galaxy evolution to be traced directly by mass as distinct from light. To date, datasets on kinematics of high-redshift galaxies contain few galaxies and the results have been somewhat discrepant. For instance, Rix et al. (1997), Simard & Pritchett (1998) find significant luminosity evolution for their low to intermediate ( $0.2 < z < 0.4$ ) redshift galaxies while Vogt et al. (1996; 1997) find evidence for only modest brightening for their ( $0.1 < z < 1$ ) sample. Apart from measuring offsets from the local TF, examining differences in the slope of the TF is also crucial (e.g. Barton et al. 2001). For instance Ziegler et al. (2002) report that the TF slope changes with redshift. An increase in the TF slope with redder passbands going from  $L_{\text{UV}}^3$  in the optical to  $L_{\text{UV}}^4$  in the near infrared has also been found (e.g. Verheijen 2001).

The discovery by COBE of an extragalactic infrared background with an intensity at least as large as that of the optical background suggests that a significant fraction of the star formation in the Universe takes place in dust enshrouded regions and is thus missed by optical surveys. With the advent of the Infrared Space Observatory (ISO, Kessler et al. 1996) deep mid-IR surveys for distant galaxies have been successfully carried out for the

first time. Operating in the  $5 - 18 \mu\text{m}$  band sensitive to warm dust and PAH/UIB emission features, ISOCAM on board ISO was more than 1000 times more sensitive than IRAS and thus had the potential to study infrared bright galaxies at redshifts beyond 0.5. A number of cosmological surveys have been performed with ISOCAM especially in the LW3 filter ( $12 - 18 \mu\text{m}$ ) resulting in the detection of galaxies down to flux density limits of  $100 \mu\text{Jy}$ . We are engaged in a followup effort to investigate the nature of galaxies discovered through deep ISOCAM surveys. This new population of galaxies is at  $z \sim 1$  and shows strong cosmological evolution (Elbaz et al. 1999, Franceschini et al. 2001). In Rigopoulou et al. (2000), (hereafter Paper I) we addressed the issue of the energetics by studying the properties of a sample of galaxies detected by ISOCAM observations of the Hubble Deep Field South (HDFS, hereafter ISOHDFS galaxies). Based on our low resolution near infrared (rest-frame R-band) spectra we concluded that ISOHDFS galaxies are powerful dusty starbursts, consistent with their large mid-IR luminosities. These observations indicate that this population traces an important phase of galaxy evolution. The next and most challenging step is to investigate their mass content and to compare it with the ongoing rate of star formation quantified in Paper I.

In this paper we present our results on spatially resolved rotation curves of four ISOHDFS galaxies selected from the sample of ISOCAM detections in the Hubble Deep Field South. We compare their properties to those of local galaxies and investigate the offset from the local TF. We find that one of the four galaxies studied is a **massive spiral with an extraordinarily high mass of  $10^{12} M_{\odot}$** .

## 2. Sample Selection

The ISOCAM observations of the Hubble Deep Field South (HDFS, Oliver et al. 2002), Aussel et al. in preparation) were carried out with two broad-band filters, LW2 ( $5-8 \mu\text{m}$ ,  $\lambda_{eff} = 6.75 \mu\text{m}$ ) and LW3 ( $12-18 \mu\text{m}$ ,  $\lambda_{eff} = 15 \mu\text{m}$ ). The ISOCAM observations were centered on the HST-WFPC2 field extending over 25 sq. arcmins, details of the observations can be found in Oliver et al. (2002). In the following we will only consider the LW3  $15 \mu\text{m}$  sample.

Oliver et al. (2002) and Aussel et al. (in preparation) analyzed the data using two independent methods. Aussel et al. used the PRETI method (Starck et al. 1999) which is based on a wavelet analysis of the combined spatial and temporal observable space. The LW3 observations resulted in the detection of 63 sources reaching down to a limiting flux of  $\sim 100 \mu\text{Jy}$  (from the analysis of Aussel et al. 2002). For our followup studies we selected objects from the Aussel et al. analysis based on the following criteria: a) a reliable LW3 detection, b)  $H_{\alpha}$  in the wavelength range of the ISAAC spectrometer (Z, SZ, J, H and K

bands) and, c) a secure counterpart in the I band image and/or a counterpart in the K band image (EIS Deep, daCosta et al. 1998). We did not apply any selection based on colors. Based on these criteria our ISOCAM HDFs (hereafter ISOHDFS) sample contains about 25 galaxies with  $15\ \mu\text{m}$  flux densities ranging between 100–800  $\mu\text{Jy}$  and provides a fair sampling of the strongly evolving ISOCAM population near the peak of the differential source counts (Elbaz et al. 1999). Near-infrared (rest-frame R-band) and optical (rest-frame B-band) low resolution spectra for our ISOHDFS sample have been presented in Paper I and in Franceschini et al. (2002).

From our ISOHDFS sample we selected randomly a few candidate objects for the high resolution studies presented here. In Table 1 we present the target’s coordinates and the available ground based photometric data (AB magnitudes) from the ESO–EIS Deep Survey (daCosta et al. 1998). The coordinates of the galaxies have been taken from Franceschini et al. (2002). In Table 2 we present morphological type (from the work of Lanzetta et al. , see footnote number 7) redshifts and  $\text{H}\alpha$  flux values (from Rigopoulou et al. 2000), LW3 fluxes and extinction estimates (from Franceschini et al. 2002) and target sizes as measured from the HDF-S WFPC2 image and/or the EIS-K band image. *The properties and morphological types of the candidate galaxies are representative of the properties of the entire sample of ISOCAM galaxies (for a discussion of the morphologies of ISOCAM galaxies see section 7).*

### 3. Data

#### 3.1. Acquisition and Reduction

We took the galaxy spectra presented here during 2000, August 20–24, and 2001, August 29–30 using the near-infrared spectrometer ISAAC (Moorwood 1998) on the ANTU–ESO telescope (formerly UT1), on Paranal, Chile. For the observations we used the medium resolution grating  $R_s \sim 5000$  and a  $0.6'' \times 2'$  long slit. The orientation of the slit was along the major axis of ISOHDFS 27 (PA:  $49^\circ$ ) and along the two nuclei in ISOHDFS 25 (PA:  $65.5^\circ$ ) (as determined from HST WFPC2 images for ISOHDFS 27 and near-IR images for ISOHDFS 25). For the observations of ISOHDFS 55 we positioned the slit at  $52^\circ$  so as to include the bright spot SE of the nucleus (the rotation curve has been corrected for the difference between the PA of the slit and the major axis). The total on-source integration time was 10800 sec for each galaxy with individual exposures being 300 sec long. Observations were done by nodding the telescope  $\pm 20''$  along the slit to facilitate sky subtraction. Sky conditions were excellent throughout the acquisition of the ISOHDFS 27 and ISOHDFS 25 spectra, with seeing values in the range  $0.25''$ – $0.6''$  while the ISOHDFS 55 spectrum was acquired through less optimal conditions (seeing  $\sim 0.8''$ ). Following the acquisition of the galaxy spectra observations we

observed spectroscopic standard stars in order to flux calibrate the galaxy spectra.

We reduced the ISAAC data using standard applications from the IRAF<sup>6</sup> package. We took spectra in nod-along-the slit pairs. To remove sky background (including OH lines) we subtracted the two frames of a pair and flat-fielded the result. We wavelength calibrated our frames using neon-argon arc-lamp frames. We then removed hot/bad pixels from the sky, star and science frames and corrected for the curvature of the slit. We transformed each exposure onto a linear wavelength grid with the dispersion axis parallel to detector rows. The sky-subtracted, co-added galaxy spectra were further divided by the spectrum of the spectroscopic standard star in order to correct for atmospheric transmission. Finally we extracted galaxy spectra using *apall* from the *twodspec* package of IRAF.

### 3.2. Light profiles

The galaxy luminosity profiles were measured using ELLIPSE in the STSDAS/ISOPHOTE package which fits isophotal ellipses to the galaxy luminosity profiles. The fits for ISOHDFS 27 and ISOHDFS 55 were made using the  $I_{814}$  image and are shown in Figure 1. The dashed lines are exponential profile fits, the disk-scale lengths are reported in Table 3. Since ISOHDFS 25 is outside of HDFS WFPC2 and flanking fields we did not have any high resolution imaging data.

### 3.3. Kinematic Modelling

To derive the rotation velocities of the galaxies as a function of position, we fit Gaussian profiles to the strongest emission line  $H_{\alpha}$ . We performed Gaussian fits using the application NGAUSSFIT within the IRAF/STSDAS package. The background was removed prior to applying the Gaussian fits. The widths were constrained to a physically meaningful value (1–20 Å). To increase the signal-to-noise ratio (S/N) of ISOHDFS 55 we smoothed the raw data by a boxcar filter of  $0.65''$  along the spatial axis before the measurement.

Determining the true rotational velocity  $V_{rot}$  of high- $z$  galaxies is, unlike the case for local spirals, far from trivial. For one, the sizes of high- $z$  galaxies are typically similar to the slit widths ( $\sim 0.6''$ – $1''$ ) so the resultant spectrum is an integration over the galaxy’s intrinsic

---

<sup>6</sup>IRAF is distributed by the National Optical Astronomy Observatories, which are operated by the Association of Universities for Research in Astronomy, Inc. under the cooperative agreement with the National Science Foundation.

velocity fields. Various methods have so far been used to measure rotational velocities in distant galaxies including seeing modelling of the emission lines (e.g. Vogt et al. 1996, 1997), a maximum-likelihood technique based on properties of local galaxies (e.g. Rix et al. 1997) or a synthetic rotation curve (e.g. Simard and Pritchett 1999, Ziegler et al. 2002).

To interpret our data we constructed a simple synthetic rotation curve (RC). We used an exponential disk to model the surface brightness distribution. The equation:

$$S(r) = S_o e^{-r/r_d}$$

where  $S_o$  and  $r_d$  are the central surface brightness and scale length of the disk, describes the surface brightness as a function of radius. In reality the surface brightness profiles of galaxies are influenced by dust absorption, however, we do not consider these effects in the present model. Although one of the galaxies studied here, the spiral ISOHDFS 27 most likely includes a bulge, our model does not include a bulge component since (a) our observations indicate that the emission lines originate in the disk, (b) bulge-disk deconvolution showed that the contribution of the bulge is much smaller than the disk and (c) we prefer to use as few model parameters as possible. We assumed that the model velocities rise linearly with radius up to one disk scale length and become flat (constant velocity) at larger radii (Persic & Salucci 1991, PS). Simard & Pritchett (1998) who used a slightly different velocity field (a step function “flat” rotation curve) in their model, found no difference between their velocity field and the PS velocity field. We computed the radius at which the intrinsic velocity flattens from the disk scale lengths  $r_d$  measured in the F814W band keeping in mind that the scale length of the younger stellar population is larger than that of the older stellar population, (Ryder & Dopita 1994). This intrinsic one-dimensional velocity field was then used to generate a 2D velocity field taking into account inclination and position angle. We measured inclination angles from HST/WFPC2 F814W images for the two galaxies ISOHDFS 27 and 55 and from the EIS K-band image for ISOHDFS 25. The errors on the measured inclination angles are small of the order of  $\pm 2^\circ$  for ISOHDFS 27 and 55 and  $\pm 5^\circ$  for ISOHDFS 25. We then convolved our disk with the appropriate Gaussian to account for the seeing and extracted a simulated Rotation Curve (RC) from the 2D velocity field by integrating over the slit aperture. The only free parameter in our model is the true rotation velocity  $V_{rot}$ . We varied  $V_{rot}$  until the extracted RC best matched the observed one. We then adopted this  $V_{rot}$  value as the true rotational velocity of the galaxy. Errors in  $V_{rot}$  were estimated by varying the inclination and position angle of each galaxy by a small amount ( $\pm 12^\circ$ ) and using the extreme values.

## 4. Results

Table 2 gives the fitting data for the galaxies studied here. Throughout this work we have assumed  $H_0 = 70 \text{ km s}^{-1} \text{ Mpc}^{-1}$ ,  $\Omega_M = 0.3$ ,  $\Omega_\Lambda = 0.7$ . The galaxies have been corrected for extinction using the Balmer decrement (Franceschini et al. 2002), and internal extinction following the prescription by Tully & Fouqué (1985).

The extracted spectra of the targets appear in Figures 2–4. For each galaxy we show the HST/WFPC2 (F814 filter) and/or K-band ground based image (for ISOHDFS 25) with the slit orientation drawn on it, the sky-subtracted 2-D spectra, the (observed) velocity profile and finally the observed rotation curves together with the model fits. Two of the galaxies studied here, ISOHDFS 27, and ISOHDFS 55 are large Sb type spirals<sup>7</sup> while ISOHDFS 25 is an interacting galaxy comprising two (as derived from the analysis) counterrotating galaxies. For the two Sb galaxies we performed fits to the light profiles (see section 3.2) which allowed us to derive bulge and disk parameters. The bulge-to-disk ratio is 0.07 and 0.02 for ISOHDFS 27 and ISOHDFS 55, respectively. The positions of the strong nebular lines  $H_\alpha$  and [NII] are labelled. As we will discuss in section 7 the galaxies studied here are representative of the morphologies found among the samples of ISOCAM galaxies. We next comment on the individual sources.

**ISOHDFS 27:** The  $H_\alpha$  emission is clearly spatially extended over  $\sim 4''$  (FWHM) which at the distance of ISOHDFS 27 corresponds to about  $\sim 25 \text{ kpc}$  ( $z=0.58$ ,  $1''=5.92 \text{ kpc}$ ). Two lobes are detected on each side of the  $H_\alpha$  continuum (same structure is seen in [NII]) providing evidence that the emission originates in a rotating disk. That the  $H_\alpha$  line emission originates in a disk is also supported by the characteristic double-horn shape seen in the line velocity profile. The  $H_\alpha$ /[NII] line ratio is about 3 which is typical of HII regions. This line ratio combined with the extended morphology of the  $H_\alpha$  line on the one hand and the LW3( $15\mu\text{m}$ )/LW2( $7\mu\text{m}$ ) flux ratio on the other, rules out the presence of a central AGN as the prime ionizing source (as already suggested in Paper I). An interesting aspect of the spectrum of ISOHDFS 27 is its velocity width. We have measured a peak-to-peak (p-p) velocity of  $440 \text{ km s}^{-1}$  (without correcting for inclination) which is much higher than typical widths measured in other  $z\sim 1$  galaxies (e.g. Vogt et al. 1997).

**ISOHDFS 25:** This is an interacting system at a redshift of  $z=0.58$ . The two galaxies are clearly separated in the ESO–EIS K-band image (in Table 1 we quote magnitudes, PAs and redshifts for both of them). We note that ISOHDFS 25 does not have an HST-WFPC2

---

<sup>7</sup>from the classification of K. Lanzetta and collaborators which can be found in [www.ess.sunysb.edu/astro/hdfs/wfpc2](http://www.ess.sunysb.edu/astro/hdfs/wfpc2)).

image since it is outside of the WFPC2 main/flanking fields (the ISOCAM HDFs field was slightly larger than the WFPC2 one). The separation between the two galaxies is  $2.46''$ . It is worth mentioning that ISOCAM's final resolution for the HDF maps (see Aussel et al. 1999 for a discussion) is  $3''$  so that ISOHDFS 25 is at the limit of what ISOCAM could resolve. However, no attempt was made to resolve the mid-infrared emission from the two components. Thus, as far as the MIR properties of ISOHDFS 25 are concerned we will treat it as a single object. The two counter-rotating galaxies are clearly seen in the sky-subtracted 2-D spectrum of ISOHDFS 25.  $H_\alpha$  emission is spatially extended in both galaxies with an extent of  $\sim 2$  arcsec (FWHM) corresponding to about 15 kpc at the distance of the galaxies. The  $H_\alpha$  is tilted in both galaxies which is attributed to ordered rotation. The velocity profiles are similar in shape and have a p-p velocity of  $\sim 300 \text{ km s}^{-1}$ .

**ISOHDFS 55:** This is an Sbc type spiral at  $z=0.76$ . The  $H_\alpha$  emission is clearly extended although no continuum has been detected. The spatial extent of the  $H_\alpha$  line over  $\sim 3$  arcsec (smaller than the optical extent of the galaxy) implies that the  $H_\alpha$  does not originate in centrally concentrated gas but most likely in a rotating disk (similar to ISOHDFS 27). The double-horn velocity profile gives additional evidence for the emission originating in a ring or disk-like structure. We see no nuclear  $H_\alpha$  emission. This could be due either to excess extinction in the galaxy's nucleus or to the presence of a significant older stellar population component (Moy et al. 2002, in preparation).

## 5. Dynamical Mass and the Mass-to-Light Ratio

The dynamical mass of spiral galaxies can be estimated based on the rotational velocity as a function of radius in the galactic plane. Spirals are assumed to consist of two components a flat disk and a spherical or spheroidal component which could be a central concentration, or a massive halo (e.g. Bahcall 1982). Since the gravitational potential is a linear function of mass, it is clear that the actual  $M(R)$  is intermediate between what would be predicted for a purely flat and a purely spherical model for the distribution of mass and the observed rotational velocity. The dynamical mass can be estimated from:

$$M(R) = \frac{fV_{obs}^2 R}{G \sin^2 i} \quad (1)$$

where  $G$  is the gravitational constant,  $i$  is the inclination of the system,  $R$  is the radius within which the mass is estimated and  $f$  is a constant which has a value between 0.5 (for a disc with a flat RC) and 1.0 (for spherical distribution) independent of the presence of a massive halo (Lequeux 1983). The formula is valid for any galaxy (in equilibrium) supported by rotation. For a disc with a flat rotation curve  $f=0.6$  while for a spherical distribution (e.g.



a galaxy dominated by a dark halo)  $f=1.0$ . For a disc with a Keplerian decreasing rotation curve outside  $R$ ,  $f=0.5$ . Thus, according to this model, for any rotating galaxy  $f$  should lie in the range:  $f=0.5$  to  $1.0$ , independent of the presence of a massive halo. Of course, the mass estimate provided by Eq. (1), will only be a good approximation of the true dynamical mass if the galaxy is supported by rotation. If on the other hand the galaxy is mainly supported by random motions, the estimated mass will be a severe underestimate. For the present mass estimates we have assumed the most realistic spherical distribution, i.e.  $f=1.0$ . In addition to the intrinsic uncertainties of this model, mass estimates of high-redshift objects suffer from additional uncertainties such as estimating the extent of the object, the inclination etc.

In Table 3 we list masses for the four ISOCAM galaxies. With a mass of  $10^{12}M_{\odot}$  (within 20 kpc) ISOHDFS 27 is clearly a very massive galaxy. Its mass is higher than that of UGC 12591 (the most massive local galaxy, (Giovanelli et al. 1986), that of L451 (a massive disk galaxy at  $z=1.34$ , van Dokkum & Stanford 2001) and the masses of other high- $z$  galaxies from the studies of Vogt et al. (1996, 1997), Moorwood et al. (2000) and Pettini et al. (2001). ISOHDFS 27 together with L451 are examples of well formed massive disk systems at  $z>0.5$ . The mass of ISOHDFS 27 corresponds to about seven times the mass of an early type galaxy at the knee of the luminosity function (Loveday 2000, Cole et al. 2001) and this is comparable to giant ellipticals and hosts of luminous QSOs and radio galaxies.

In Figure 5 we investigate the correlation between dynamical mass and bolometric luminosity for the ISOHDFS galaxies presented here, and compare it to that for local spirals (M33, M51), luminous and ultra-luminous IR galaxies (LIRGS, ULIRGs, NGC 6240, NGC 3256, Arp 220) and the prototypical starburst galaxy M82. We also plot  $M/L_{bol}$  values for spirals and elliptical galaxies. We list the mass-to-light ratio for the ISOHDFS galaxies in Table 3. The bolometric luminosities of the ISOHDFS galaxies have been extrapolated from their MIR luminosities assuming  $L_{FIR}/L_{MIR} \sim 10$  (Roussel et al. 2001) and, assuming  $L_{FIR} \sim L_{bol}$ . The dynamical masses for the ISOHDFS galaxies can be found in Table 3, those for the remaining galaxies have been taken from the literature. We note that for the purpose of the plot in Figure 5 ISOHDFS 25 is treated as a single object (see explanation in section 4). The ratio  $M/L_{bol}$  has been estimated assuming the mass of *both* components, for the  $L_{bol}$  the  $L_{MIR}$  has been used. To estimate the  $M/L_{bol}$  value for elliptical galaxies we used the Bruzual & Charlot models (Bruzual & Charlot 1993) to compute the fraction  $L_B/L_{bol}$ , assuming  $M/L_B \sim 16$  (e.g. Schweizer et al. 1989). We find that  $L_B/L_{bol} \sim 0.4$  therefore,  $M/L_{bol} = 6.5$ . The value is in agreement with the  $M/L_{bol} \sim 5$  measured by Arnaud & Gilmore (1986). For the spirals we used the  $M/L_{bol} \sim 3.0$  (e.g. Burbridge & Burbridge 1975).

The mean  $M/L_{bol}$  ratio for ISOHDFS 25 and ISOHDFS 55 is 0.5, close to the value found for the IR luminous starbursting galaxy NGC 3256 (0.3). ISOHDFS 27 on the other hand,

has an  $M/L_{bol}$  ratio of 2.4, similar to the value for M51. It is evident from Figure 5 that, the  $M/L_{bol}$  ratio is higher for earlier Hubble types. Starburst activity however, influences the  $M/L_{bol}$  ratio, since bursts increase the luminosity resulting in lower  $M/L_{bol}$  ratios. Since the three galaxies are representative examples of the entire ISOCAM population we conclude that the  $M/L_{bol}$  ratio of the majority of ISOCAM galaxies is not as low as in local infrared luminous starburst galaxies but rather between the values for massive IR luminous starburst galaxies akin to NGC 3256 and large normal spirals. ISOHDFS 27 represents the small fraction of ISOCAM galaxies ( $\sim 10\%$ ) that are large early type spirals whose large MIR luminosity is mostly due to their large masses.

## 6. Tully-Fisher Relation

In order to look for kinematic evidence of luminosity evolution in high redshift galaxies one can compare the kinematical properties of high- $z$  galaxies to those of local galaxies. Tully & Fisher (1977) showed that there exists a good correlation between HI line width and galaxy luminosity, the so-called Tully-Fisher (TF) relation. Although the original TF was established using velocity widths measured in HI which sample the full galactic disks, Simard & Pritchett (1998) and Courteau (1997) showed that there is a tight correlation between measured HI and  $H_\alpha$  rotation velocities so that internal kinematics measured from the  $H_\alpha$  should also follow the same TF as the HI.

In Figure 6 we compare the present data of the ISOCAM galaxies with the local rest-frame B-band Tully-Fisher (TF) relation of Pierce & Tully (1992, PT). The rest-frame B-band data correspond approximately to observed R-band at  $z \sim 0.6$  and I-band at  $z \sim 0.8$ . The PT relation used data for 16 galaxies from the Ursa Major Cluster to define the calibration and six local galaxies to define the zero-point. The relation is described by:

$$M_B = -7.48 (\log W_R - 2.50) - 19.55$$

where  $M_B$  is the total B-magnitude and  $W_R$  is the width of the HI line corrected for inclination and turbulence following the prescriptions of Tully & Fouqué (1985). In Figure 6 we plot the inverse TF fit i.e.,  $V_{rot}$  as a function of absolute magnitude  $M_B$ . We have converted the PT observed linewidths  $W_R$  to rotational velocities following the method of Simard & Pritchett (1998). We corrected the rotational velocities for the effects of instrumental broadening,  $(1+z)$  cosmological redshift effect,  $\sin i$  inclination and, finally for extinction. Since ISOCAM galaxies have been selected from deep MIR surveys extinction plays a crucial role. We have estimated the extinction in the optical  $A_V$  based on measurements of the Balmer decrement for a subsample of the entire ISOHDFS sample. In general we find

that the  $A_V$  varies between 1.2–2.0 mag (Franceschini et al. 2002). To correct the present data we have used the “conservative”  $A_V$  value of 1. Using the data for the four galaxies (for the purpose of the TF plot we have plotted both components of ISOHDFS 25 using the available magnitudes and the velocities measured from the present work) we compute a weighted offset of  $1.66 \pm 0.28$  mag relative to the local B-band relation.

However, the B-band PT relation may not be the most appropriate for comparison to the present ISOCAM sample since the B-band is more sensitive to star formation and extinction. Hence, we have compared our ISOCAM data also to the I-band PT relation defined as ( from Pierce & Tully 1992):

$$M_I = -8.72 (\log W_R - 2.50) - 20.94$$

where  $M_I$  is the total I-band magnitude and  $W_R$  as before. We note that rest-frame I-band data correspond to observed J-band at  $z \sim 0.6$  and H-band at  $z \sim 0.8$ . The I-band is more sensitive to the underlying older stellar population and is less affected by extinction. In Figure 7 we show the comparison of the kinematical data for ISOCAM galaxies to the I-band PT relation. We compute a weighted offset of  $0.7 \pm 0.26$  mag relative to the local I-band relation. **Although our sample is very small for statistically significant results, a clear offset from the local TF is evident in both the rest-frame B and I bands.**

A number of data-sets have so far appeared in the literature which, based almost exclusively on *rest-frame B-band spectroscopy*, have successfully probed the TF relation at moderate redshifts. The results can be grouped in two categories: those finding evidence for significant luminosity evolution (e.g. Koo et al. , 1995, Rix et al. , 1997, Simard & Pritchett 1998) and those finding modest (or no) evolution (e.g. Vogt et al. 1996, 1997). More recently, Barden et al. (in preparation), studied the kinematics of a sample of [OII]-bright objects at  $0.7 < z < 1.5$  (based on  $H_\alpha$  rotational curves) and found significant luminosity evolution increasing with redshift. The present sample of ISOCAM galaxies differs from all previous ones since it is primarily a mid-IR selected sample. For the selection of our objects we have not imposed any criteria based on emission-line strengths, sizes, and inclination. However, the high star-formation rates found ubiquitously among ISOCAM objects (Paper I) implies that our galaxies are in fact strong  $H_\alpha$  emitters although for the kinematical study we did not preselect based on  $H_\alpha$  strengths.

The differences in the luminosity evolution found among the various groups implies that sample selection is in fact crucial. The galaxies in the studies of Koo et al. (1995) sample the low-end of galaxy masses. Most of their objects are compact bright emission line galaxies. They find evidence for brightening up to 4 mags. The samples of Rix et al. (1997) and Simard & Pritchett (1998) sample larger galaxies (scale-lengths of about 2

kpc) and luminosities in the range  $L^*$  to sub- $L^*$ . They find evolution of about 1.5 mag. Vogt’s (1996, 1997) samples include even larger galaxies (scale lengths  $>3$  kpc) and the resulting brightening is modest of the order of 0.4 mag. The present ISOCAM galaxies are large (scale lengths 7–9 kpc) and show strong  $H_\alpha$  emission.

Can these conflicting findings be somehow reconciled? The answer is yes and to explain the apparent discrepancy one has to assume that the luminosity evolution is highly dependent on the masses/sizes of the galaxies. In this scenario the low-mass(/small size) galaxies show substantial luminosity evolution as they undergo interactions/merging and their kinematics are more susceptible to local phenomena such as supernovae winds and outflows. On the other hand the massive (/large size) galaxies are less susceptible to interactions thus their luminosity shows less variation in comparison to low-mass(/small size) galaxies. Another possibly crucial parameter is the galaxy morphology (i.e. along the Hubble sequence). Although the current samples of high- $z$  galaxies are not large enough to allow morphological investigations, studies of local samples (e.g. Rubin et al. , 1982, 1985) indicate that there is a variation in the kinematical properties of galaxies according to their morphological types. However, issues of internal absorption corrections are indeed important as discussed by Kodaira & Watanabe (1988). Finally, the emission-line strength also plays a role: higher luminosity evolution is expected in objects which are undergoing (or have recently undergone) episodes of star-forming activity compared to the more quiescent ones.

How do the present results compare with previous studies? From the above discussion it is obvious that the only meaningful comparison is with the samples of Vogt et al. (1996, 1997). Despite the fact that both samples contain large (in size) galaxies we measure a higher luminosity evolution than that found by Vogt et al. The measured offset is bound to increase if we use a higher extinction value  $A_V$  for the present ISOCAM galaxies. Taken at face value the difference in the luminosity evolution found between the two samples seems to contradict the mass-dependent luminosity evolution scenario. However, this is not the case: as we mentioned earlier, emission-line bright objects show a higher luminosity evolution than the more quiescent ones. A significant difference between the present ISOCAM sample and the Vogt samples, is that the former has been drawn from a parent sample of strong  $H_\alpha$  emitters (Paper I). The Vogt et al. galaxies were selected from a magnitude limited sample for having emission line flux extending beyond the nuclear regions (so that the rotation curves could be traced out to the disk). However, this selection criterion does not bias the sample towards emission-line bright objects. In fact, the few Vogt et al. galaxies, for which we have been able to find published Keck spectra in the literature (e.g. Forbes et al. 1996), are rather weak [OII]-emitters. We conclude that selection criteria are important when studying TF at high-redshifts and that the existence of a mass and emission-line strength dependent luminosity evolution is probably the cause of the differences found by the various groups.

## 7. ISOCAM Galaxies and Implications for the IR Extragalactic Background

With the availability of very deep source counts and upper limits on the diffuse isotropic emission at shorter wavelengths the Extragalactic Background Light (EBL) has been reasonably constrained at visible, IR and submm wavelengths. The contribution of known galaxies to the optical EBL has been calculated by integrating the emitted flux times the differential number counts down to the detection threshold. Madau & Pozzetti (2000) showed that the optical EBL is dominated by a large number of relatively faint galaxies at  $z \simeq 0.7$  with almost negligible contributions from the luminous Lyman Break Galaxies (e.g. those observed by Steidel et al. (1996)) .

The discovery by COBE of an infrared EBL (e.g. Puget et al. 1996, Fixsen et al. 1998, Finkbeiner, Davis & Schlegel 2000) with an intensity similar to or greater than that of the optical EBL has generated a lot of interest in identifying the infrared galaxies responsible for it. The infrared EBL peaks around  $\lambda \sim 140 \mu\text{m}$ . It is thus interesting to investigate the relative contributions of the newly detected ISOCAM galaxies to the infrared EBL. Elbaz et al. (2002) carried out detailed calculations of the relative contributions of various types of objects such as luminous infrared starbursts, AGN, and normal galaxies to the infrared EBL. With luminosities greater than  $10^{10} L_{\odot}$  at  $8.5 \mu\text{m}$  (in the rest frame), a median redshift of 0.75, and bolometric luminosities between 2 and  $10 \times 10^{11} L_{\odot}$ , ISOCAM galaxies are in fact LIRGs. Based on their calculations, Elbaz et al. (2002) find that the contribution of ISOCAM galaxies to the peak of the infrared EBL can be of the order of 50% or more, (i.e. a significant fraction) dependent of course on the exact shape of the underlying spectral energy distribution.

Once we have established that ISOCAM galaxies are major contributors to the infrared EBL, it is interesting to investigate the properties of these galaxies and compare them to the properties of the galaxies responsible for the optical EBL. The discovery of four massive ISOCAM galaxies has prompted us to take an in-depth look at into the morphologies of both the present ISOHDFS galaxies and the ISOCAM detections in HDF-N (Aussel et al. 1999, Moy et al. in preparation). For the identification of the optical/near-IR counterparts of the ISOHDFS galaxies we have used the WFPC2/F814W image and/or the EIS K-band image (da Costa et al. 1998). Out of the ISOCAM sample of 63 galaxies we were able to find secure identifications for up to 90% of them (about 58 sources, for the remaining sources there is either no ground-based imaging followup and/or there was no clear counterpart). About half of the sources with optical/near-IR counterparts, appear to be interacting systems similar to ISOHDFS 25 while the remaining objects appear to be large disk dominated spirals like ISOHDFS 55 (scale length of 7 kpc) or as large as ISOHDFS 27 (scale length 11 kpc about  $\sim 10\%$  of ISOHDFS galaxies). Aussel et al. (1999) reached similar conclusions for the HDF-

N. Although we do not have estimates of the dynamical mass for the majority of ISOHDFS galaxies, Franceschini et al. (2002) presented baryonic mass estimates for a large fraction of ISOHDFS galaxies. Based on their estimated baryonic masses and the dynamical mass estimates presented here, we conclude that ISOHDFS galaxies are indeed massive galaxies. Both ISOCAM samples (HDF-N & S) show star formation rates of the order of 30–100  $M_{\odot}yr^{-1}$  as deduced from their MIR luminosities (e.g. Franceschini et al. 2002).

Since the ISOHDFS galaxies presented here are representative of the morphologies and properties of the galaxies of the entire ISOCAM sample we suggest that the infrared EBL is probably dominated by these few (in numbers), large or interacting galaxies and massive IR luminous galaxies, as opposed to the smallish but more numerous faint blue galaxies that were found to contribute to the optical EB (Madau & Pozzetti 2000). Thus the objects that contribute to the IR EB are not the standard IR counterparts of normal spiral and irregular galaxies but are IR luminous ( $L > \text{few} \times 10^{11} L_{\odot}$ ), massive ( $M > \text{few} \times 10^{11} M_{\odot}$ ) galaxies with median redshift 0.7.

## 8. Conclusions

We have presented first results from internal kinematic studies of four intermediate redshift ( $z = 0.6 - 0.8$ ) galaxies detected by ISOCAM in the HDFs. The kinematics are derived from high resolution spatially resolved  $H_{\alpha}$  velocity profiles. The galaxies studied, two large Sbc spirals and a double pair/interacting system, are representative of the morphologies of the entire ISOHDFS sample. Our results are summarized as follows:

ISOHDFS galaxies tend to be massive galaxies with masses of a few  $\times 10^{11} M_{\odot}$ . One of the galaxies studied, ISOHDFS 27, contains a mass of  $10^{12} M_{\odot}$  (within 20 kpc) substantially higher than the masses measured in other intermediate redshift galaxies and, comparable to the mass of giant ellipticals and hosts of luminous QSOs and radio galaxies. The presence of a central AGN in this galaxy is ruled out by three independent pieces of evidence: the extend/ morphology of the  $H_{\alpha}$  emission, the  $H_{\alpha}/[NII]$  ratio of 3 (typical of starbursts) and the mid-infrared  $LW3(15\mu m)/LW2(7\mu m)$  ratio which again is typical of values found in local luminous IR galaxies. Based on the MIR luminosities and assuming  $L_{FIR} = 10 L_{MIR}$  we have calculated the mass-to-light ratio  $M/L_{bol}$  of ISOHDFS galaxies. The  $M/L_{bol}$  values are between the values found for local IR luminous star-forming galaxies and massive spirals.

We have compared the four ISOCAM galaxies to the local B and I-band Tully-Fisher relations. We have measured offsets of  $1.6 \pm 0.3$  and  $0.7 \pm 0.3$  mag from the B and I-band TF relations, respectively. Although our sample is very small to draw statistical conclusions it is

evident that a clear offset from the local TF relations exist. We discuss the possible existence of a mass-dependent luminosity evolution where small mass (size) galaxies are more likely to undergo merging/interactions and thus show substantial luminosity evolution. In addition, recent episodes of star-forming activity, thus strong emission-line objects, are bound to show higher luminosity evolution than the more quiescent ones. Overall, we find that selection effects are very crucial to studies of the TF relation in intermediate/high redshift systems. We stress the uniqueness of our sample (an infrared selected one), when comparing it to other studies.

We have examined the global morphological properties of the ISOHDFS galaxies: 40% of ISOHDFS galaxies are double pair/interacting systems (akin to ISOHDFS 25), with the remaining being field disk-dominated spirals (similar to ISOHDFS 55). A further  $\sim 10\%$  of the spirals are large early-type systems like ISOHDFS 27. Based on the current dynamical mass estimates and estimates of the baryonic masses for the majority of the ISOHDFS galaxies we find that ISOCAM galaxies are indeed massive systems. Our results imply that the IR background is dominated by a small number of massive and IR luminous star-forming galaxies near  $\langle z \rangle \sim 0.7$ .

We acknowledge support from the European Community RTN Network "POE" (under contract HPRN-CT-2000-00138). We appreciate discussions with Michael Rowan-Robinson regarding dust extinction and William Vacca regarding modelling of stellar populations.

## REFERENCES

- Arnaud K.A., Gilmore, G. 1986, MNRAS, 220, 759
- Aussel, H., Elbaz, D., Cesarsky, C.J., Stark, J.L. 1999, in *The Universe as seen by ISO*, eds. P. Cox, M.F. Kessler, ESA SP 47, 1023
- Bahcall, J.N., Schmidt, M., Soneira, R.M. 1982, ApJ, 258, 17
- Barton, E.J., Geller, M. J., Bromley, B. C., van Zee, L., Kenyon, S. J. 2001, AJ, 121, 625
- Bruzual, A.G., Charlot, S. 1993, ApJ, 405, 538
- Burbidge, E.M., & Burbidge, G.R. 1975, in *Galaxies and the Universe*, p. 81, eds Sandage, A.R., Sandage, M. & Kristian, J., University of Chicago press.
- Cole, S., Norberg, P., Baugh, C.M., et al. 2001 MNRAS, 326, 255

- Courteau, S. 1997, AJ, 114, 2402
- da Costa, L.N., et al. 1998, preprint (astro-ph/9812105)
- Elbaz, D., Cesarsky, C.J., Fadda, D., et al. 1999 A&A, 351, L37
- Elbaz, D., Cesarsky, C.J., Chaniai, P., Aussel, H., Franceschini, A., Fadda, D., Chary, R.R. 2002, A&A, 384, 848
- Faber, S.M., & Jackson, R.E. 1976, ApJ, 204, 668
- Feast, M.W., & Robertson, B.S.C. 1978, MNRAS, 185, 31
- Finkbeiner, D.P., Davis, M., Schlegel, D.J. 2000, ApJ, 544, 81
- Fixsen, D.J., Dwek, E., Mather, J.C., Bennett, C.L., Shafer, R.A. 1998, ApJ, 508, 123
- Forbes, D., Phillips, A.C., Koo, D.C., Illingworth, G.D. 1996, ApJ, 462, 89
- Franceschini, A., Aussel, H., Cesarsky, C.J., Elbaz, D., Fadda, D. 2001, A&A, 378, 1
- Franceschini, A., et al. 2002, A&A, submitted
- Giovanelli, R., Haynes, M.P., Rubin, V.C., Kent, W.F. 1986, ApJ, 301, L7
- Gronwall, C., & Koo, D.C. 1995, ApJ, 440, 1
- Kessler, M.F., Steinz, J.A., Anderegg, M.E. 1996, A&A, 315, 27
- Kodaira, K., Watanabe, M. 1988, AJ, 96, 1593
- Koo, D.C., & Kron, R.G. 1992, ARA&A, 30, 613
- Koo, D.C., Guzman, R., Faber, S.M., et al. 1995, ApJ, 440, L49
- Kormendy, J., McClure, R.D. 1993, AJ, 105, 1793
- Lanzetta, K., et al. the classification catalogue is available at  
<http://www.ess.sunysb.edu/astro/hdfs/wfpc2>
- Lequeux, J. 1983, A&A, 125, 394
- Lilly, S., et al. 1995, ApJ, 455, 108
- Loveday, J. 2000, MNRAS, 312, 557
- Madau, P., & Pozzetti, L. 2000, MNRAS, 312, L9



- McLeod, K.K., Rieke, G.H., Rieke, M.J., Kelly, D.M. 1993, *ApJ*, 412, 111
- Mo,H.J., Mao, S. 2000, *MNRAS*, 318, 163
- Moorwood, A.F.M. 1998, *Msngr*, 74, 7
- Moorwood A.F.M., van der Werf, P.P., Cuby, J.G., Oliva, E. 2000, *A&A*, 362, 9
- Navarro, J.F., Steinmetz, M., 2000 *ApJ*, 538, 477
- Oliver, S., Mann,R.G., Carballo,R., et al. 2002, *MNRAS*, 332, 536
- Persic, M., & Salucci, P. 1991, *ApJ*, 368, 60
- Pettini, M., et al. 2001, preprint(astro-ph/0102456)
- Pierce, M.J., & Tully, R.B. 1992, *ApJ*, 387, 47 (PT)
- Puget, J.-L., Abergel, A., Bernard, J.-P., et al. 1996, *A&A*, 308, 506
- Rigopoulou, D., et al. 2000, *ApJ*, 537, 85 (Paper I)
- Rix, H.-W., Guhathakurta, P, Colless, M., Ing, K. 1997, *MNRAS*, 285, 779
- Roussel, H., Sauvage, M. Vigroux, L. Bosma, A. 2001, preprint(astro-ph/0104088)
- Rubin, V.C., Thonnard, N., Ford, W.K.,Jr., Burstein, D. 1982, *ApJ*, 261, 439
- Rubin, V.C., Burstein, D., Ford, W.K. Jr., & Thonnard, N. 1985, *ApJ*, 289, 81
- Ryder, S.D., Dopita, M.A. 1994, *ApJ*, 430, 142
- Sakamoto, K., Scoville, N.Z., Yun, M.S., et al. 1999, *ApJ*, 514, 68
- Schweizer, F., van Gorkom, J.H., Seitzer, P. 1989, *ApJ*, 338, 770
- Simard,L., Pritchett,C.J. 1998, *ApJ*, 505, 96
- Simard,L., Pritchett,C.J. 1999, *PASP*, 111, 453
- Steidel, C.C., Giavalisco, M., Pettini, M., Dickinson, M., Adelberger, K.L. 1996, *ApJ*, 462, L17
- Tecza, M., Genzel, R., Tacconi, L.J., et al. 2000, *ApJ*, 537, 178
- Thronson, H.A., & Greenhouse, M.A. 1988, *ApJ*, 327, 671

- Tully, R.B., & Fisher, J.R. 1977, *A&A*, 54, 661
- Tully, R.B., & Fouqué, P. 1985, *ApJS*, 58, 67
- van Dokkum, P.G., & Stanford, S.A. 2001, preprint(astro-ph/0110153)
- Verheijen, M.A.W. 2001, *ApJ*, 563, 694
- Vogt, P.N. et al. 1996, *ApJ*, 465, L15
- Vogt, P.N., et al. 1997, *ApJ*, 479, L121
- Ziegler, B.L., Bohm, A., Fricke, K.J., et al. 2002, *ApJ*, 564, 69

## FIGURES

Fig. 1.— Surface Brightness profiles

Fig. 2.— HST/WFPC2 image–2D spectrum–  $H_\alpha$  velocity profile– rotation curve for ISO-HDFS 27

Fig. 3.— ESO-EIS image–2D spectrum–  $H_\alpha$  velocity profile– rotation curve for ISOHDFS 25

Fig. 4.— HST/WFPC2 image–2D spectrum–  $H_\alpha$  velocity profile– rotation curve for ISO-HDFS 55

Fig. 5.— M/L ratio

Fig. 6.— B-band Tully–Fisher

Fig. 7.— I-band Tully–Fisher

Table 1. Photometric data

Obj	RA (J2000)	Dec (J2000)	U <sup>1</sup>	B <sup>1</sup>	V <sup>1</sup>	R <sup>1</sup>	I <sup>1</sup>	J <sup>1</sup>	H <sup>1</sup>	K <sup>1</sup>
S27	22 32 47.71	-60 33 35.3	22.2	21.9	21.00	20.1	19.5	18.9	18.39	18.17
S25NE	22 32 45.73	-60 32 25.6	24.1	23.4	22.7	21.9	21.4	20.27	19.80	19.58
S25SW	22 32 45.62	-60 32 26.1	24.4	23.6	23.0	22.0	21.6	20.68	20.24	19.76
S55	22 32 58.01	-60 32 33.8	23.8	23.5	22.7	22.0	21.3	20.6	20.05	19.88

<sup>1</sup>magnitudes in the AB system from the EIS Deep survey (see text)

Table 2. Morphological and spectroscopic data

Obj	Type	z	Flux( $H_\alpha$ ) <sup>1</sup> $\times 10^{16} \text{erg cm}^{-2} \text{s}^{-1}$	Flux(LW3) mJy	$A_V^2$ mag	scale <sup>3</sup> kpc arcsec <sup>-1</sup>
S27	Sb	0.58	3.28	0.39	1.5	5.9
S25NE	Pair	0.58	3.12	0.47 <sup>4</sup>	1.7	5.9
S25SW	Pair	0.58	2.47	–	1.7	5.9
S55	Sbc	0.76	2.41	0.20	1.8	7.2

<sup>1</sup>observed values

<sup>2</sup> $A_V$  measured from the Balmer decrement (Franceschini et al. 2002)

<sup>3</sup>the physical scale of 1'' at the distance of the galaxy

<sup>4</sup>includes both galaxies

Table 3. Kinematic modelling data

Obj	inclination deg	$R_d$ kpc	$V_{rot}$ $\text{km s}^{-1}$	Mass(within radius) <sup>1</sup> $\times 10^{11} M_\odot$	$M/L_{bol}$ $M_\odot/L_\odot$
S27	$49 \pm 2$	11	$460 \pm 40$	10 (20 kpc)	2.2
S25NE	$65 \pm 5$	– <sup>2</sup>	$260 \pm 45$	2.3 (14 kpc)	$0.54^3$
S25SW	$65 \pm 5$	– <sup>2</sup>	$249 \pm 52$	2.1 (14 kpc)	–
S55	$52 \pm 2$	7	$270 \pm 75$	2.1 (14 kpc)	0.50

<sup>1</sup>mass within the extent of the rotation curve

<sup>2</sup>no scale length has been estimated (object lies outside of HDF-S WFPC2 and FF)

<sup>3</sup>includes both galaxies

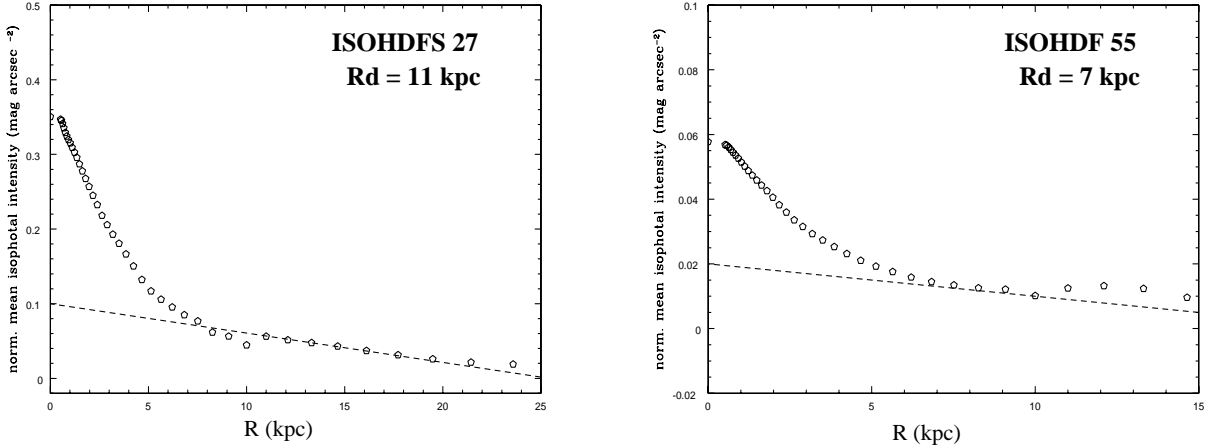


Fig. 1.— Radial normalised intensity profiles (in magnitudes arcsec<sup>-2</sup>) for the two galaxies ISOHDFS 27 and ISOHDFS 55 which fall within the WFPC2 image. The profiles have been determined with STSDAS/ELLIPSE. The dashed line is the exponential disk fit.

Fig. 2.— ISOHDFS 27, from top left clockwise: HST/WFPC2  $I_{814}$  -band image (North up, East to the left), near-IR VLT–ISAAC 2D spectrum,  $H_\alpha$  velocity profile, and rotation curve. The ISAAC slit width and orientation are indicated on the WFPC2 image. The points in the velocity curve represent the observed velocities and the solid line is the model rotation curve.

Fig. 3.— ISOHDFS 25, from top left clockwise: ESO–EIS Deep K -band image, near-IR VLT–ISAAC 2D spectrum,  $H_\alpha$  velocity profile, and rotation curve. In the  $H_\alpha$  velocity profile plot: ISOHDF S25–NE component is represented by a solid line, ISOHDFS 25–SW component by dotted line. In the velocity curve plot, filled circles and triangles represent the observed velocities of the S25–NE and S25–SW component, respectively. Slit orientation, pixel scale and velocity curve as in Figure 2.

Fig. 4.— ISOHDFS 55, from top left clockwise: HST–WFPC2  $I_{814}$  -band image, near-IR VLT–ISAAC 2D spectrum,  $H_\alpha$  velocity profile, and rotation curve. Slit orientation, pixel scale and velocity curve as in Figure 2.

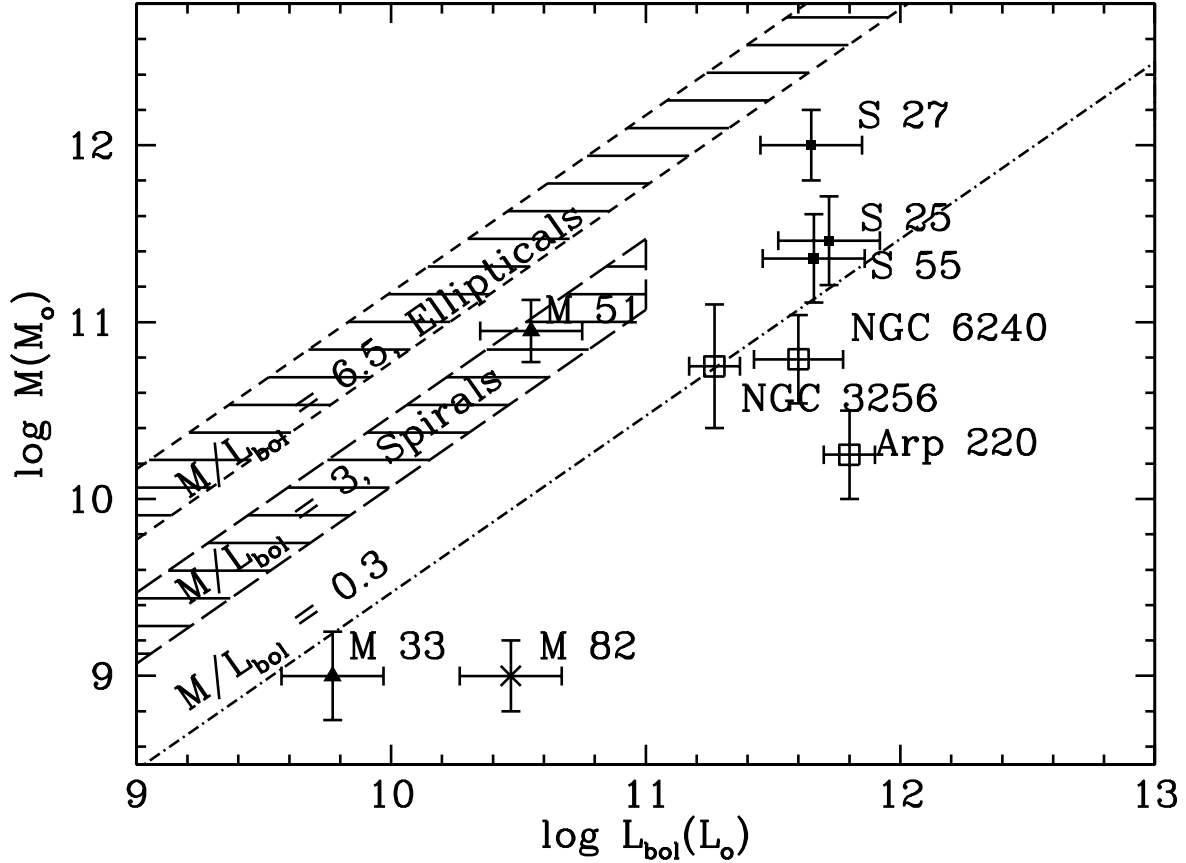


Fig. 5.— Total masses ( $r \sim 3-2$  arcsec, depending on galaxy size) in solar units vs. bolometric luminosities for our ISOHDFS galaxies (filled squares), Luminous IR galaxies (open squares), local spirals (filled triangles), starburst (cross). The regions occupied by Ellipticals ( $M/L_{bol}$ :  $6.5 M_\odot/L_\odot$ ) Schweizer et al. (1989) (see also text) and spirals ( $M/L_{bol}$ :  $3 M_\odot/L_\odot$ ) Burbridge & Burbridge (1975) are indicated. The NGC 3256 ratio of  $M/L_{bol}$ :  $0.3 M_\odot/L_\odot$  is also shown (dotted line). For the remaining objects shown the  $M/L_{bol}$  values have been taken from the literature. The areas (radii) at which  $M$  was calculated have been chosen to match the ISOCAM data. References: NGC 3256: Feast & Robertson (1978), NGC 6240: Tecza et al. (2000), Arp 220: Sakamoto et al. (1999), M 51: Thronson & Greenhouse (1988), M 33: Kormendy & McClure (1993), M 82: McLeod et al. (1993).

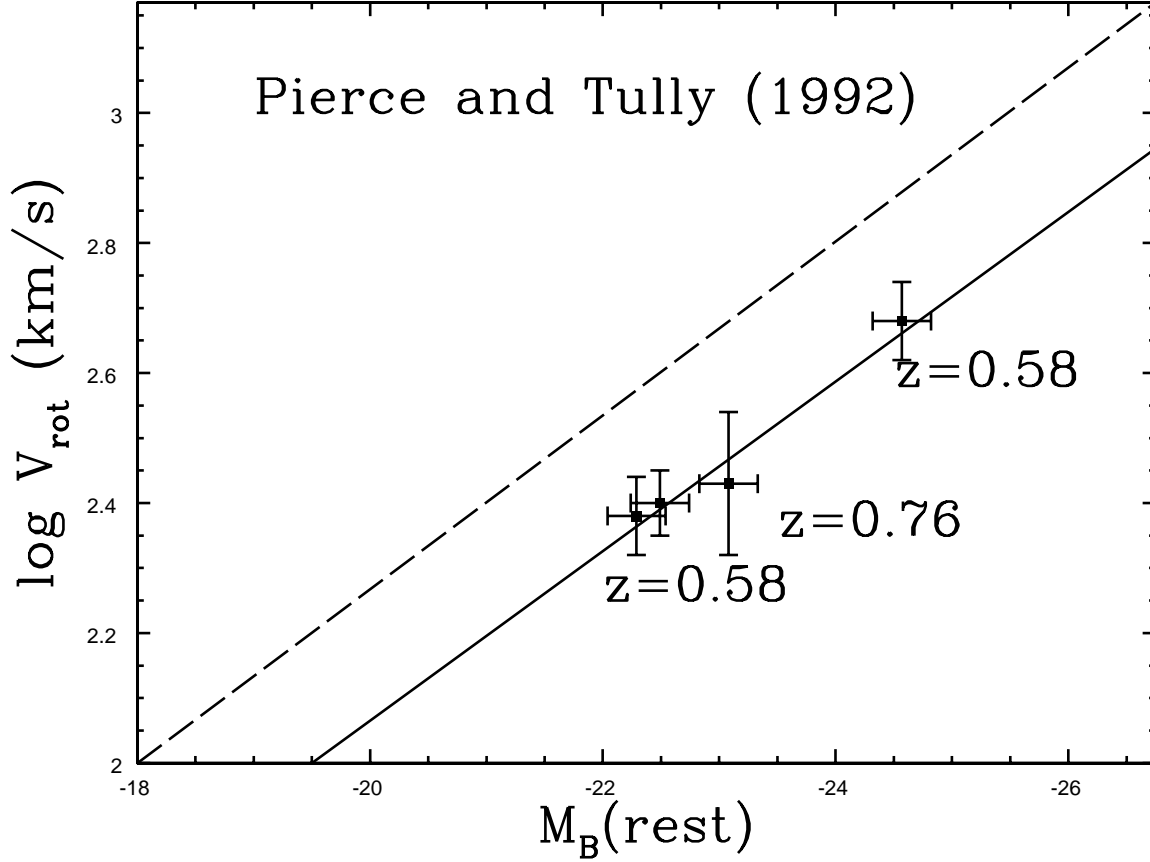


Fig. 6.— The Tully–Fisher  $V_{\text{rot}}$  as a function of  $B_{\text{rest}}$  luminosity diagram. Our ISOCAM data are compared to the local TF by Pierce and Tully (1992, dotted line). The magnitudes have been corrected for internal extinction and the velocities for projection. The straight line is the fit to the ISOCAM points assuming same slope as the local TF. We find an offset of  $1.6 \pm 0.3$  from the local TF relation.



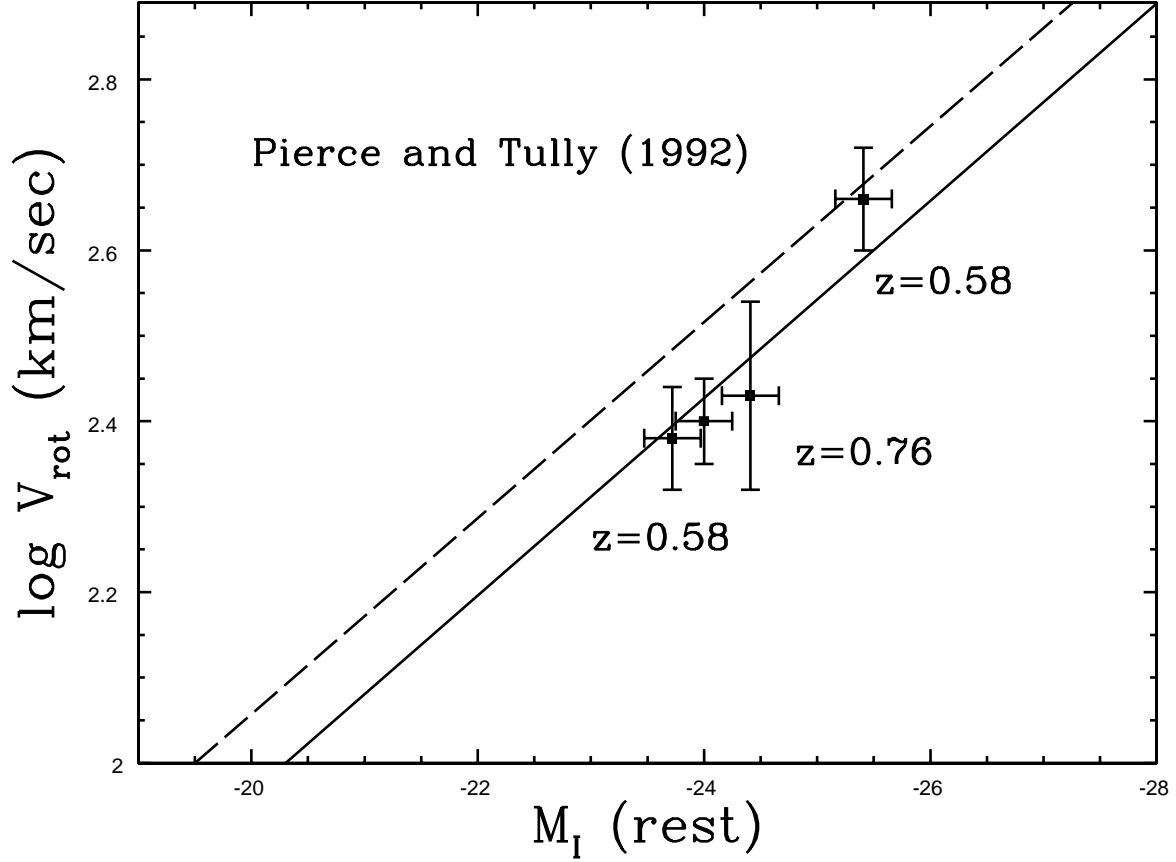


Fig. 7.— The Tully–Fisher  $V_{\text{rot}}$  as a function of  $I_{\text{rest}}$  luminosity diagram. Our ISOCAM data are compared to the local TF by Pierce and Tully (1992, dotted line). The magnitudes have been corrected for internal extinction and the velocities for projection. The straight line is the fit to the ISOCAM points assuming same slope as the local TF. We find an offset of  $0.7 \pm 0.26$  from the local TF relation.

This figure "f2.jpg" is available in "jpg" format from:

<http://arxiv.org/ps/astro-ph/0207457v1>

This figure "f3.jpg" is available in "jpg" format from:

<http://arxiv.org/ps/astro-ph/0207457v1>

This figure "f4.jpg" is available in "jpg" format from:

<http://arxiv.org/ps/astro-ph/0207457v1>